Carbon 127 (2018) 329–339

Contents lists available at ScienceDirect

Carbon

journal homepage: www.elsevier.com/locate/carbon

Preparation mechanism of hierarchical layered structure of graphene/copper composite with ultrahigh tensile strength

Ziyue Yang [a], Lidong Wang [a, *], Zhendong Shi [a], Miao Wang [a], Ye Cui [b], Bing Wei [c], Shichong Xu [d], Yunpeng Zhu [e], Weidong Fei [a, e, **]

[a] School of Materials Science and Engineering, Harbin Institute of Technology, Harbin, 150001, China
[b] College of Materials Science and Chemical Engineering, Harbin Engineering University, Harbin, 150001, China
[c] Department of Materials Science and Engineering, South University of Science and Technology of China, Shenzhen, 518000, China
[d] Key Laboratory of Functional Materials Physics and Chemistry of the Ministry of Education, Jilin Normal University, Siping, 136000, China
[e] School of Mechanical Engineering, Qinghai University, Xining, 810016, China

ARTICLE INFO

Article history:
Received 16 July 2017
Received in revised form
29 September 2017
Accepted 23 October 2017
Available online 2 November 2017

ABSTRACT

Nacre-like composite is promising to realize the intriguing properties of graphene in metal matrix. However, how to fabricate the composite with nacre-like structure and improve effectively its property is still challenging. Here we report a facile synthesis of reduced graphene oxide(RGO)/copper(Cu) composite with hierarchical layered structure based on molecular level mixing and self-assembly. The effects of pH value, temperature, mixing method and graphene content on the microstructure and mechanical property of composite were investigated. The pH value and temperature are the main factors in the formation of hierarchical layered structure. For macroscale microstructure, the composites consist of parallel carbon-rich strip aggregates and carbon-poor matrix. For microscale microstructure, the carbon-rich aggregate contains many micro-layered grains composing of alternating layers of graphene and copper, forming a nacre-like composite structure. Furthermore, it is believed that the length-width ratio of macroscopic aggregates related with the mixing method has a significant impact on the mechanical properties of composites. The tensile strength of the 2.5 vol% RGO/Cu composite is as high as 748 MPa. Moreover, good electrical conductivity is also obtained in the composites. This work provides a better understanding of design graphene based composites with hierarchical layered structure and high performance.

1. Introduction

Graphene, a two-dimensional material with a monolayer of sp^2 bonding carbon [1], has attracted intensive attention in the past decades. It has the highest known intrinsic strength of 130 GPa, a Young's modulus of 1 TPa [2–5] and high electron mobility of ~15,000 cm^2 $V^{-1}S^{-1}$ [6]. Graphene has been recognized as a promising reinforcement for polymer matrix composite [7,8] and metal matrix composite [9–11] owing to its unique two-dimensional geometry and excellent strength and modulus.

Recently, copper matrix composite reinforced with graphene has attracted great attention of researchers. By introducing graphene into copper matrix, the mechanical, electrical, thermal properties and oxidation resistance of the composites are expected to improve [10,12–15]. However, the mechanical properties of the graphene/Cu composites are still unsatisfying. One of the reasons is the aggregation of graphene in the Cu matrix. Thus the synthesis of Cu-matrix composite with uniformly dispersed graphene is still an important issue.

Shell nacre has a “brick-and-mortar” structure, which consists of 95% hard mineral aragonite “brick” and 5% soft protein “mortar” in-between. The unique structure provides a guidance for designing the structure of graphene/Cu composite. Inspired by the nacre-like structure of, Xiong et al. absorbed reduced graphene oxide (RGO) into porous Cu perform and sintered into composite [16]. The 1.2 vol% nacre-like RGO/Cu composite has a tensile strength of 308 MPa, which is 41% higher than pure Cu (218 MPa). The researchers also fabricated high content (~45 vol%) RGO/Cu

* Corresponding author.
** Corresponding author. School of Materials Science and Engineering, Harbin Institute of Technology, Harbin, 150001, China.
E-mail addresses: wld@hit.edu.cn (L. Wang), wdfei@hit.edu.cn (W. Fei).

https://doi.org/10.1016/j.carbon.2017.10.095
0008-6223/

composite with nano-laminated structure *via* bottom-up assembly, reduction and consolidation [17]. The as-obtained nano-laminated composite exhibits increased compressive strength (294 MPa) and well recoverable deformation ability compared with the pure Cu. However, the mechanical properties of the composites mentioned above are still lower than the expectation. Kim et al. fabricated a nanolayered composite which consists of alternating layers of graphene and copper [14], which was similar to the nacre-like structure. It is astonishing to find that the nanolayered graphene/Cu composite has an ultra-high compressive strength of 1.5 GPa. However, the entire process used in the nanolayered composite is too complicated to fabricate bulk material, which limits its application.

Molecule level mixing (MLM) is a promising method to produce CNT [18] and graphene reinforced copper composites [19], which can achieve good mechanical property by a facile process. Hwang et al. first achieved the uniform dispersion of RGO and Cu matrix by molecular level mixing process; the ultimate tensile strength of 2.5 vol% RGO/Cu is 325 MPa [19]. Chen et al. investigated the effect of graphene content on the microstructure and properties of Cu matrix composites; lower graphene content (no more than 0.8 vol %) benefited to its strengthening effect in the composites [20]. Despite the dispersion improvement achieved by MLM method, it is difficult to entirely avoid the agglomeration of graphene in Cu matrix and further improve the strength of composite.

In our previous study, we have successfully fabricated a graphene-copper composite with micro-layered structure based on the MLM method and confirmed that the micro-layered structure has a significant impact on the microstructure and property of RGO/Cu composite [21]. During the MLM process, the micro-layered structure was spontaneously formed driven by van der Waals force and hydrogen bonding. Thank for the micro-layered structure of RGO/Cu composite, the tensile strength of the composite with 5 vol% RGO is as high as 608 MPa. However, we have only a superficial understanding of the microstructure of the RGO/Cu composite, which needs to be further studied. Moreover, optimizing experimental condition and exploring the formation mechanism of micro-layer structure in the composite are also necessary.

Here, we report a facile synthesis of graphene/copper composite with hierarchical layered structure and ultrahigh strength, which is a continuation of our previous work on the graphene/copper composites. The hierarchical structure contains both parallel carbon-rich strip aggregates in macroscope and many micro-layered grains composing of alternating layers of graphene and copper in microscope, which is constructed by a self-assembly method and controlled by the pH value and temperature during the MLM process. High shear mixing can increase the length-width ratio of strip aggregates and improve the mechanical properties of composites. This work will provide a better understanding of the configuration design of graphene/copper composite and contribute to optimize its mechanical property.

2. Experimental

2.1. Fabrication of pure copper powder and RGO/Cu composite powders

Graphene oxide (GO) colloid provided by Zhejiang C6G6 Technology Co., Ltd., was diluted with deionized water and treated by sonicating for 30 min to form a uniform suspension (1 mg/ml). A certain amount of GO suspension was dispersed into 2000 ml aqueous solution of $Cu(CH_3COO)_2 \cdot H_2O$ (115.9 g). Then 4 M NaOH aqueous solution was added into the above mixed solution dropwise. And the obtained slurry was allowed to be further stirred for 20 min. After that the slurry was centrifuged and rinsed with deionized water before being dried at 110 °C for 4 h under vacuum to obtain a powder. Finally, the powder was reduced in H_2—Ar gas, whose H_2 concention in Ar is 17 vol%, at 400 °C for 5 h to obtain RGO/Cu composite powder. For comparison, pure copper powder was also prepared. 115.9 g of $Cu(CH_3COO)_2 \cdot H_2O$ powders were dispersed into 2000 ml deionized water to form an aqueous solution. 4 M NaOH aqueous solution was added into the $Cu(CH_3COO)_2 \cdot H_2O$ aqueous solution under high-shear mixing with a rotating speed of 3000 rpm at 20 °C until the pH value was 13.6. The drying and reduction process was preformed exactly the same as the above composite powder.

The effects of the volume fraction of RGO, the reaction temperature, the pH value and the mixing method during the MLM process on the microstructure and properties of the composites were studied; in each set of experiments, one parameter was changed while the others remain constant. For simplification, the composites were abbreviated as αG/Cu-β°C -pH$\gamma(\theta)$; α vol% corresponds to the volume fraction of RGO and sets as 2.5, 5 or 7.5 vol%, respectively, adopting the density of graphene oxide as 2.3 g/cm^3; β °C is the reaction temperature and sets as 20, 40 or 50 °C, respectively; pH γ is the pH value during MLM process and sets as 5.9, 6.6, 12.8 or 13.6, respectively; θ represents the mixing method: mechanical stirring abbreviated as "S" achieved by stirring paddles with the rotating speed of 200 rpm, and high-shear mixing abbreviated as "H" achieved by a rotor-stator mixer (JRJ300-1) with the rotating speed of 3000 rpm.

2.2. Consolidation of the pure copper powder and the RGO/Cu composite powders

The as-prepared pure copper powder and RGO/Cu composite powders were sintered by spark plasma sintering (SPS, SPS-1050) at 600 °C for 5 min under vacuum with a heating rate of 75 °C/min and a sintering pressure of 40 MPa. The size of the obtained RGO/Cu composite was 30 mm in diameter and 5 mm in thickness.

2.3. Characterizations

The atomic force microscopy (AFM) image was taken by a Ben Yuan CSPM 5600 scanning probe microscope in a tapping mode. The sample of graphene oxide for AFM imaging was prepared by dropping graphene oxide solution on natural mica for 30 s and dried in 50 °C for 4 h. The microstructures of the composite powders and consolidated composites were observed by scanning electron microscopy (SEM, Helios Nanolab600i) equipped with an energy-dispersive X-ray spectrometer (EDS) and transmission electron microscopy (TEM, Talos F200x). The composite sample for etching experiment was polished with diamond polishing slurry after mechanical polishing with 3000-grit SiC paper, immersed in $FeCl_3$ solution for 1 min and rinsed with 10 vol% HCl solution. X Ray Diffraction (XRD) analysis was performed on a Philips X'Pert X-ray diffractometer with Cu K_α radiation ($\lambda = 1.54$ Å). The surface charge properties of composite particles were evaluated by a Zetasizer Nanoseries-ZS90 (Malvern) instrument. The samples were diluted with HCl or NaOH solution at a constant pH value. The zeta potential of each sample was measured three times, and the average value was calculated.

Tensile tests were performed on an electronic universal testing machine (Instron-5569) under a crosshead speed of 0.5 mm/min. The test samples were a dog-bone shape with a gauge length of 15 mm, width of 2 mm and thickness of 1 mm. The electrical resistivities of the composites were measured by direct current low resistance test instrument from Suzhou Changsheng Technology Co. The testing directions of the samples in tensile and electrical conductibility tests were both perpendicular to the processing

direction during sintering.

3. Results and discussion

3.1. Microstructure characterizations of graphene oxide

Fig. 1a shows an SEM image of GOs after freeze drying. The GO flakes have a transparent and corrugated structure without agglomeration. AFM can be used to measure the thickness of GO flakes. An individual GO flake can be found in Fig. 1b with the thickness of ~0.9 nm, which is the typical monolayer thickness of graphene oxide [3].

3.2. Microstructure characterizations of composite powders

In order to clarify the synthesis process of the composite powders, pH-dependent experiments were carried out, during which the samples were taken at different pH values of 5.9, 6.6, 12.8 and 13.6, respectively. XRD patterns of the as-collected samples are shown in Fig. 2a. It is necessary to note that all the composite powders here were freeze dried to eliminate the effect of drying temperature on their microstructure and present their original state in the solution. It shows that the phase constitution of the composite powders is pH-sensitive. When the pH value is lower than 6.6, the diffraction peaks are assigned to the crystal planes of $Cu_2(OH)_3Ac$ (PDF 50-0407) [22]. However, once the pH value is increased to 12.8, the major diffraction peaks match well with $Cu(OH)_2$ and CuO. It indicates that $Cu_2(OH)_3Ac$ was formed at the initial stage of dropping NaOH solution and gradually transformed into $Cu(OH)_2$ and CuO with the further increasing amount of hydroxyl ions.

Fig. 2b–e shows the morphology change of the composite powders at various pH values as indicated by SEM analysis. As shown in Fig. 2a and b, $Cu_2(OH)_3Ac$ is in the form of sheet and about 5 μm in size in acidic media (pH 5.9 and 6.6), which combines well with GOs. When pH value is increased to 12.8 and 13.6, the $Cu_2(OH)_3Ac$ sheets transform into $Cu(OH)_2$ and CuO nanofibers. The nanofibers are uniformly dispersed on GO sheets with diameters of a few tens of nanometers. More importantly, the edges of GO sheets can be easily observed and almost parallelly distributed, which can be considered the framework of micro-layered composite particles.

To further clarify the formation mechanism of the micro-layered composite particles, we investigated their surface charges by zeta potential measurements. The zeta potential is a physical property exhibited by any particle in dispersion and is an important parameter used for evaluating the dispersion degree or aggregative trend in dispersing media. It is well known that particles whose zeta potentials are more positive than +30 mV or more negative than −30 mV are considered to achieve stable and uniform dispersions due to interparticle electrostatic repulsion [23]. Fig. 2f shows the zeta potential of the composite particles at various pH values. At the initial stage, the zeta potential of composite particles increases with increasing pH value and the highest value reaches to 45 mV at pH 7. The composite particles achieve stable dispersion in the pH range of 5.9–9. However, as the pH value further increases to 12.8, zeta potential of composite particles decreases dramatically and remains around −10 eV. It indicates that the solution system is unstable in the pH range of 9–13.6.

It is found that the reaction temperature has an impact on the copper compound in the composite powders during MLM process. Fig. 3a shows the XRD patterns of the composite powders prepared at 20 °C, 40 °C and 50 °C while the pH value is kept at 13.6. It can be found that the composite powders prepared at 20 °C and 40 °C exhibit the characteristic peaks similar with the standard $Cu(OH)_2$ (PDF 80-0656) and CuO (PDF 80-1917). However, the composite powders prepared at 50 °C only exhibit the characteristic peaks corresponding to CuO. The XRD results suggest that higher reaction temperature would make the intermediate product $Cu(OH)_2$ dehydrate into CuO completely. For simplification, the composite powders are abbreviated as GO/CuO_xH_y and CuO_xH_y represents CuO ($x \neq 0$ and $y = 0$) or a mixture of CuO and $Cu(OH)_2$ ($x \neq 0$ and $y \neq 0$).

Fig. 3b–d presents the morphology of the composite powders fabricated at various temperatures. As shown in Fig. 3b, the copper compound in the heat-dried composite powder (20 °C) has a sheet-like structure of about 500 nm in size, which is different from the nanofiber structure in the freeze-dried composite powders. The reason may be that during vacuum drying process the nanofibers are aligned *via* "oriented attachment" [24,25]. The paralleled nanofibers assemble with each other and finally form into nanosheets [26]. Moreover, these nanosheets exhibit homogeneous distribution without any agglomeration. When the reaction temperature is increased to 40 °C, the nanosheets in composite powders are much smaller and are about 200–300 nm in size. However, when the temperature reaches to 50 °C, many tiny nanorods with diameter of a few tens of nanometers instead of nanosheets can be observed. In addition, the nanoparticles obtained at 40 °C and 50 °C are severely agglomerated, which can be ascribed to their high surface energy and strong Van der Waals force.

3.3. Characterizations of composites

In order to study the microstructure of RGO/Cu composite, XRD, XPS and SEM measurements were carried out. Fig. 4a shows the XRD pattern of the 2.5G/Cu–20C-pH13.6(H) composite sintered by SPS process. The composite exhibits only three characteristic peaks

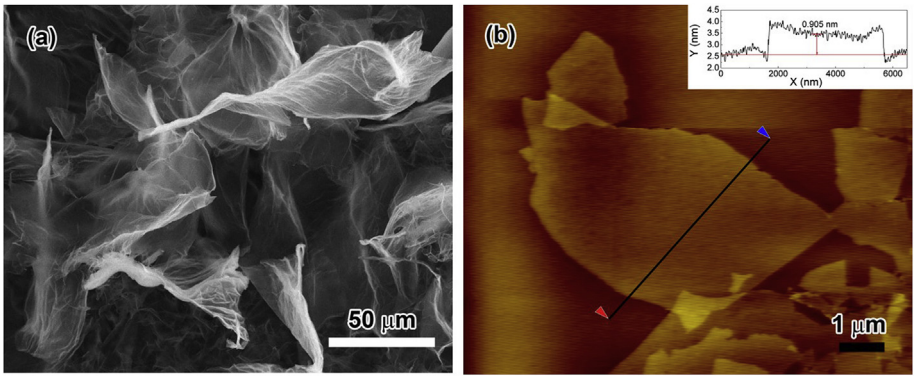

Fig. 1. (a) SEM image of the GO flakes, (b) AFM image of the GO flakes. (A colour version of this figure can be viewed online.)

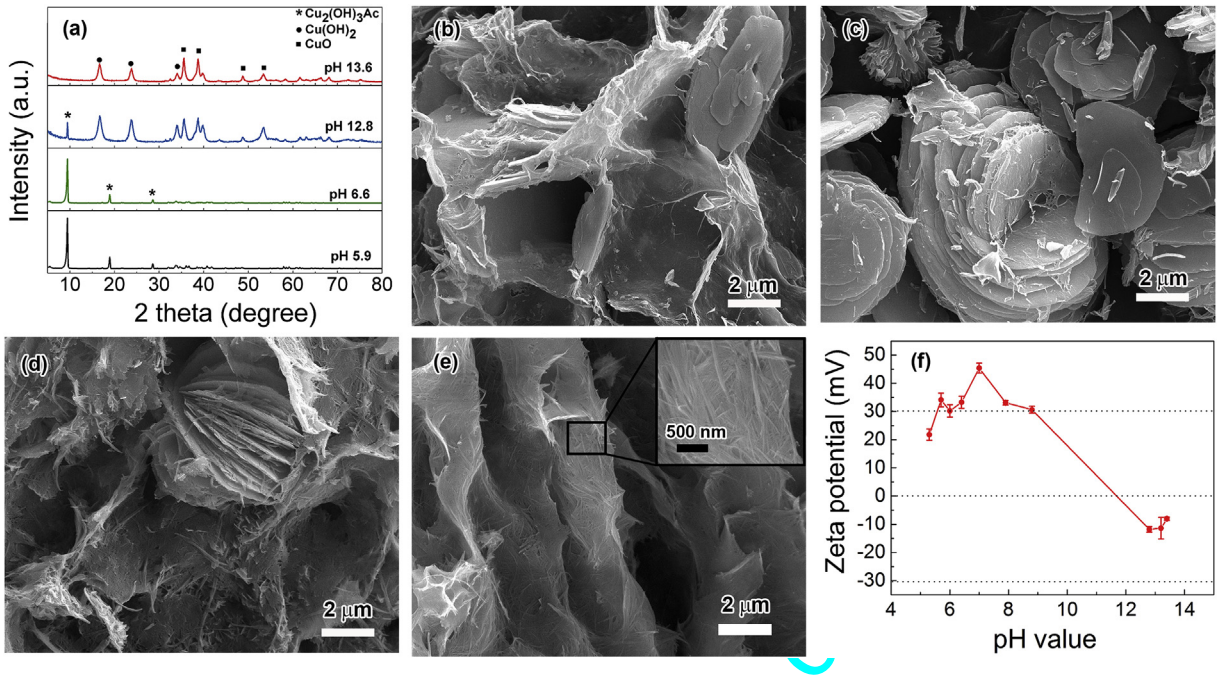

Fig. 2. (a) XRD patterns of freeze-dried composite powders fabricated at various pH values, SEM images for freeze-dried composite powders fabricated at (b) pH 5.9, (c) pH 6.6, (d) pH 12.8, (e) pH 13.6, (f) Zeta potential of the composite powders fabricated at various pH values. (A colour version of this figure can be viewed online.)

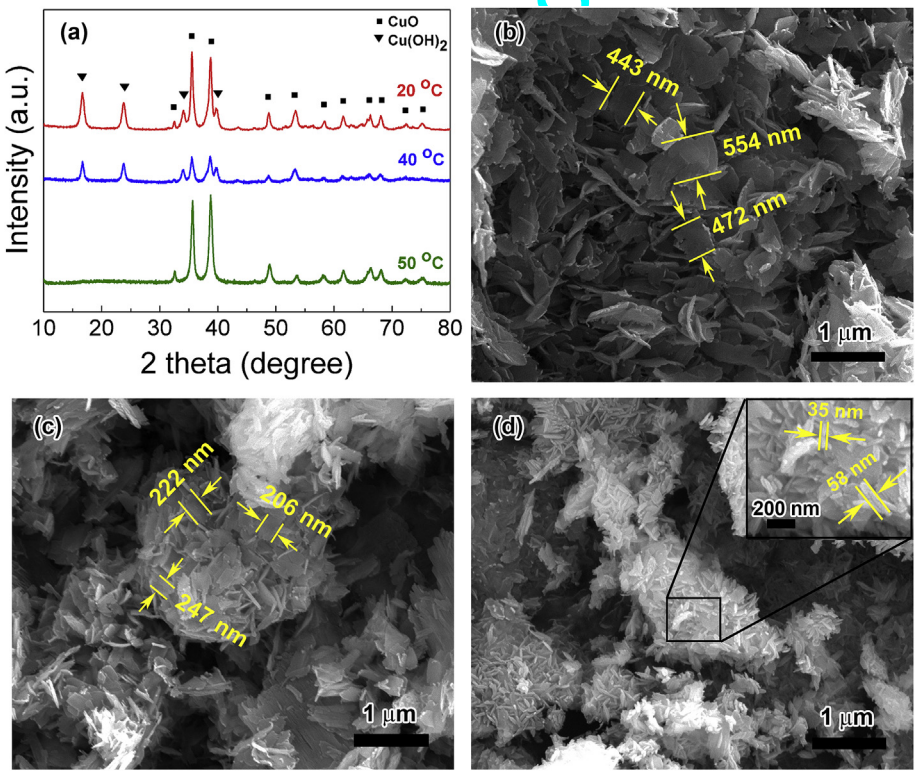

Fig. 3. (a) XRD patterns of the composite powders prepared at various reaction temperatures and dried in vacuum at 110 °C, SEM images of the composite powders prepared at (b) 20 °C, (c) 40 °C and (d) 50 °C. (A colour version of this figure can be viewed online.)

corresponding to Cu (PDF No.851,326), which suggests that copper matrix was not oxidized during the SPS process.

XPS was used to investigate chemical valence states of Cu, C and O in GO/CuO_xH_y composite powder and RGO/Cu composite. As shown in Fig. 4b, the XPS spectra of GO/CuO_xH_y composite powder and RGO/Cu composite both exhibit C 1s peak at around 284.5 eV, O 1s peak at around 531 eV, Cu LMM peak at around 570 eV, Cu $2p_{3/2}$ peak at around 932 eV and Cu $2p_{1/2}$ peak at around 951.2 eV. The elemental analysis indicates that the C content increases from 9.44% to 32.57% and O content decreases from 37.95% to 22% after

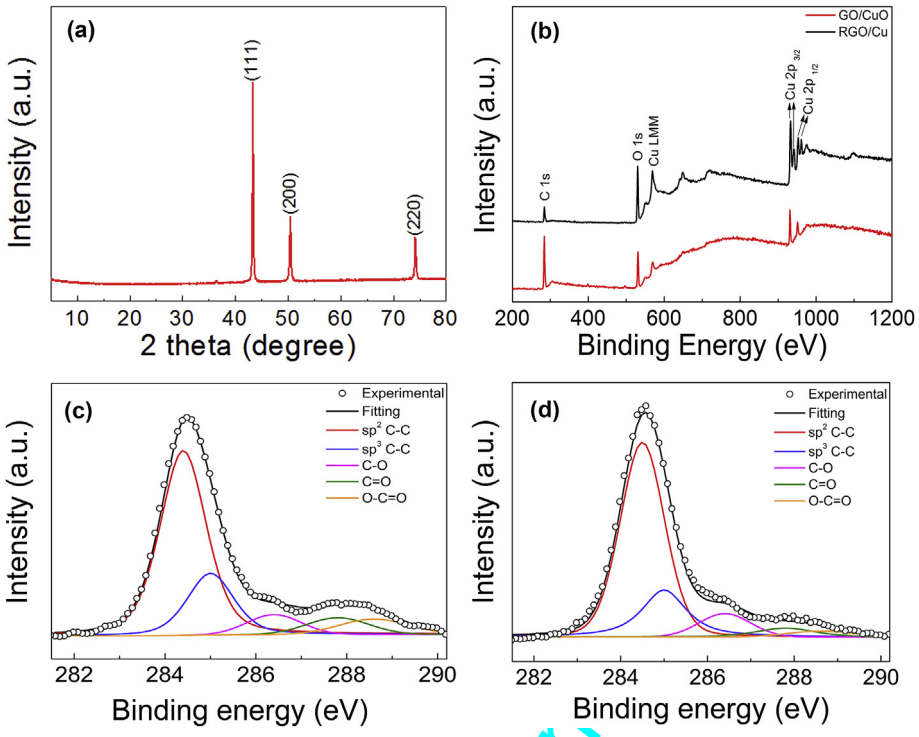

Fig. 4. (a) XRD pattern of the 2.5G/Cu-20C-pH13.6(H) composite, (b) survey XPS spectrum of GO/CuO_xH_y composite powder and RGO/Cu composite, (c) C1s XPS spectrum of GO/CuO_xH_y composite powder, (d) C1s XPS spectrum of RGO/Cu composite. (A colour version of this figure can be viewed online.)

reduction (Table 1), which confirms the reducing effect of hydrogen treatment on GO/CuO_xH_y composite powder. In fact, there are three kinds of oxygen atoms in RGO/Cu composite: one is the oxygen from residual functional groups such as carboxyl groups on the RGO sheets after reduction; the other is the oxygen atoms from Cu–O bonds at the interface between RGO and Cu matrix [19], the Cu–O bonds are generated from the interaction between the Cu ions and GO sheets, which are the origin for improving the interfacial strength between RGO and Cu [27,28]; the third is the oxygen from the copper oxides on the surface of copper powder exposed to air before SPS process.

In order to investigate the effect of the reduction process on the graphene oxide, the C1s spectra was fitted using a Gaussian-Lorentzian peak shape after performing a linear background correction. The relative atomic percentages of different carbon bonds were calculated from the corresponding peak areas in C 1s spectrum of GO/CuO_xH_y composite powder and RGO/Cu composite. As shown in Fig. 4c and d, the peak located at 284.5 eV and 285 eV are attributed to the sp^2-hybridized and sp^3-hybridized carbon atoms [29] and the small peaks at 286.4 eV, 287.8 eV and 288.6 eV originate from the C–O, C=O and O–C=O bonds [30,31], respectively. The calculate results are summarized in Table 2. It is obvious that RGO/Cu composite possesses higher percentage of sp^2-hybridized carbon, which indicates higher degree of graphitization and fewer defects in the lattice structure of graphene after reduction [32]. Furthermore, compared with GO/CuO_xH_y composite powder, the RGO/Cu composite has lower percentage of C=O and O–C=O bonds but higher percentage of C–O bond. It suggests that hydrogen reduction treatment can eliminate the C=O and O–C=O bonds and produce more C–O bonds, which may form the oxygen mediated carbon/Cu bonding (C–O–Cu bond) and enhance the bonding strength between graphene and Cu matrix [19]. Even though the relative amount of C–O bond increases, total amount of oxygen-containing groups decreases from 18.9% to 15.3%. In addition, we calculate the C/O ratio in RGO according to the relative atomic percentages of different carbon bonds calculated by fitting the C1s XPS spectrum of RGO/Cu composite. The calculated C/O ratio is 11.3:1, which is close to that in Ref. [33] (12:1). It confirms the reducing effect of hydrogen treatment on GO sheets.

Table 1
Atomic percentages of GO/CuO_xH_y composite powder and RGO/Cu composite based on XPS survey.

Sample name	Atomic percentage (%)		
	C 1s	O 1s	Cu 2p
GO/CuO_xH_y	9.44	37.95	52.61
RGO/Cu	32.57	22	45.43

Fig. 5a and b shows the SEM images displaying the cross section of etched composite fabricated by high-shear mixing and mechanical stirring. It can be seen that there are two types of phases in both composites: the dark one has a strip structure with length of 50–400 μm, whereas the light gray one is continuous. In contrast, the 2.5G/Cu–20C-pH13.6(H) composite has more dispersed phases than the 2.5G/Cu–20C-pH13.6(H). Furthermore, it seems that the morphology of the dispersed phases in the 2.5G/Cu–20C-pH13.6(H) composite is slender strip while the ones in the 2.5G/Cu–20C-pH13.6(S) composite are close to elliptical shape. Therefore, 30 pieces of dispersed phases were randomly selected in the SEM images, and their lengths and widths were measured and analyzed. The distributions of the length-width ratio of the strips in the 2.5G/Cu–20C-pH13.6(H) and the 2.5G/Cu–20C-pH13.6(S) composites are shown as histogram in the insets of Fig. 5a and b, and the average length-width ratios are 3.26 and 5.60, respectively. It can be confirmed that the high-shear mixing can produce the strip phases with larger length-width ratio than agitator stirring.

As shown in the SEM image of etched cross section of the 2.5G/Cu–20C-pH13.6(H) composite (Fig. 5c), the dark part is relatively

Table 2
Atomic percentages of different bonds of carbon calculated by fitting the C 1s spectra of GO/CuO_xH_y composite powder and RGO/Cu composite.

Sample name	Atomic percentage (%)					
	sp^2 C–C	sp^3 C–C	C–O	C=O	O–C=O	Total functional groups
GO/CuO_xH_y	61.2	19.9	6.4	6.2	6.3	18.9
RGO/Cu	64.7	20.0	8.0	4.5	2.8	15.3

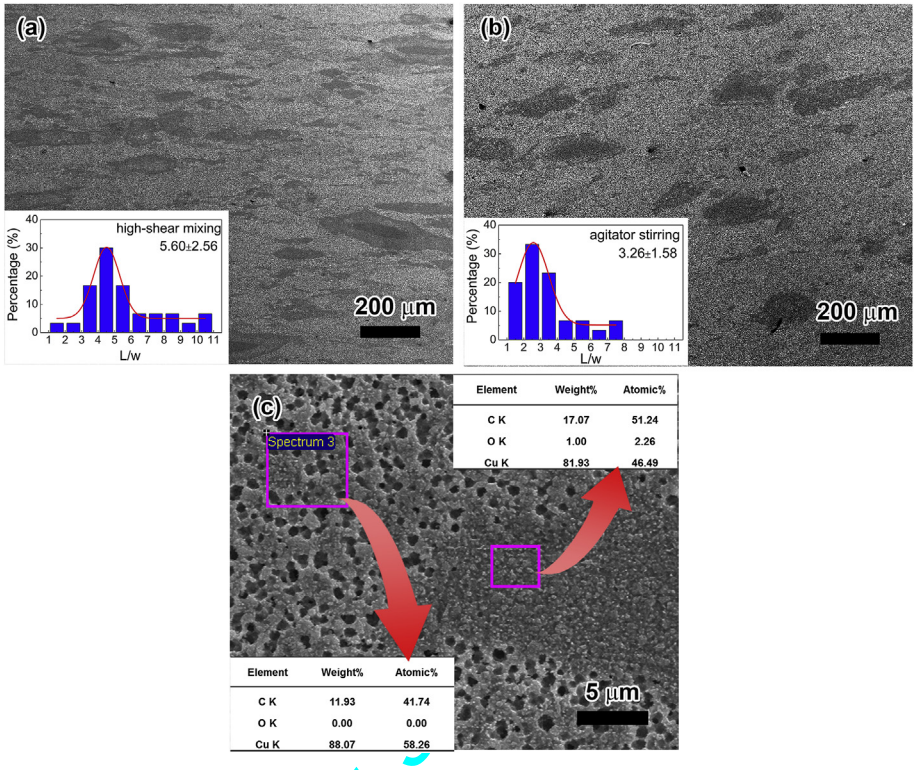

Fig. 5. (a) SEM image of etched cross section of the 2.5G/Cu-20C-pH13.6(H) composite, (b) SEM image of etched cross section of the 2.5G/Cu-20C-pH13.6(S) composite. The insets in (a) and (b) show the length-width ratio distribution of strip structure in the 2.5G/Cu-20C-pH13.6(H) and the 2.5G/Cu-20C-pH13.6(S) composites respectively, and data in the top right corner of the insets indicate mean length-width ratio and standard deviations. (c) SEM image of etched cross section of the 2.5G/Cu-20C-pH13.6(H) composite with the inserts showing the EDX analyses of the dark compacted part and light gray porous part, respectively. (A colour version of this figure can be viewed online.)

compacted while the surrounding part is porous after etching. EDX measurements are used to investigate the elemental content of the two phases in the composite. The results show that the dark phase has more carbon content compared to the light gray phase. It suggests that the two phases have different microstructure although they consist of both graphene and copper. The strip phase cannot be easily etched because plenty of graphene can hinder the flow of the etching solution [12].

According to above experimental results, we can illustrate the growth process of the hierarchical layered RGO/Cu composites as shown in Fig. 6. Firstly, for the solution of GO and $Cu(CH_3COO)_2$, since there are many oxygen-containing groups with negative charges on the surface of GO, such as hydroxyl, epoxide and carboxyl, Cu^{2+} ions are easily attracted by these functional groups on GO surface [34]. Secondly, with the addition of NaOH solution, Cu^{2+} ions react with NaOH and *in-situ* produce $Cu_2(OH)_3Ac$ sheets (as shown in Fig. 2b and c) in the pH range of 5.9–9, which flattened on the surface of GO sheet. The zeta potential of GO/$Cu_2(OH)_3Ac$ composite particles is higher than +30 eV, which is stable in the solution. With further addition of OH^- ions, $Cu(OH)_2$ and CuO can be produced in the composite particles instead of $Cu_2(OH)_3Ac$. Moreover, the copper compound produced at low temperature has a nanosheet structure, which exhibits homogeneous distribution and easily combine with GO sheets. The zeta potential of GO/CuH_xO_y composite sheets decrease below +30 eV but above −13 eV in the pH range of 9–13.6, which is unstable for the composite particles in the solution. Thus self-assemble could happen by minimizing the surface energy, the composite nanosheets are prone to stack layer by layer due to their two-dimensional plane structure and form the composite particles with micro-layered structure.

Thirdly, the micro-layered composite particles are still unstable in the solution. The subunits are prone to further assemble with each other and finally form into hierarchical layered structure during mixing and centrifugation process. However, residual composite sheets do not participate in the self-assembly but combine with the $Cu(OH)_2$ particles that precipitate from the solution. After reduction and sintering process, RGO/Cu composite with hierarchical layered structure in both macroscopic and microscopic scale is obtained. It is worth noting that high-shear mixing can produce more strip phases with larger length-width ratio than mechanical stirring, and achieve more uniform dispersion of graphene in the Cu matrix.

TEM analysis was used to further investigate the micromorphology and crystalline structure of the pure copper and 2.5G/Cu-20C-pH13.6(H) composite. Fig. 7a is a representative TEM image of

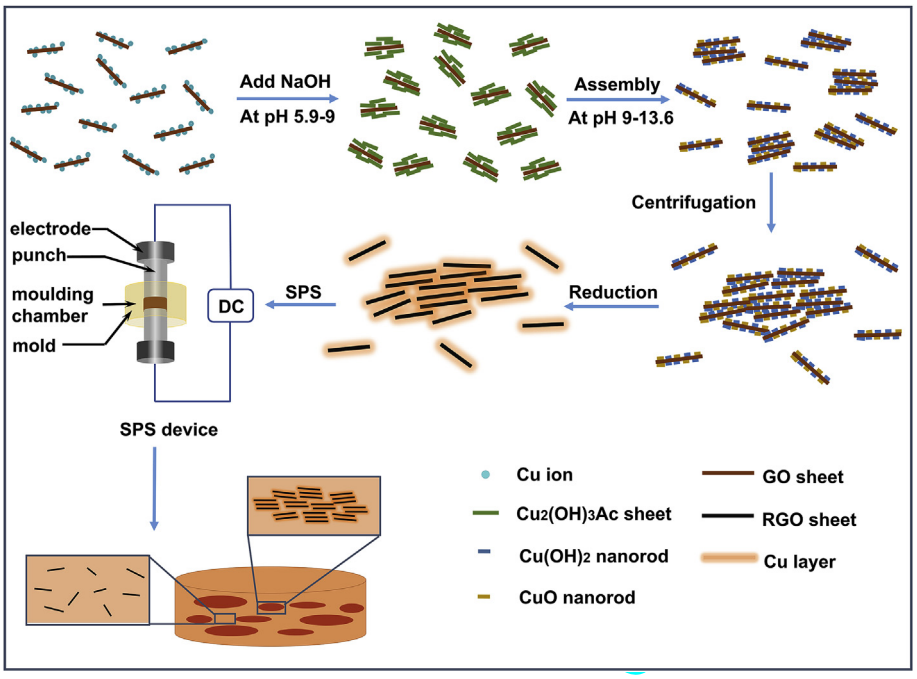

Fig. 6. Schematic illustration of the formation of hierarchical layered RGO/Cu structure. (A colour version of this figure can be viewed online.)

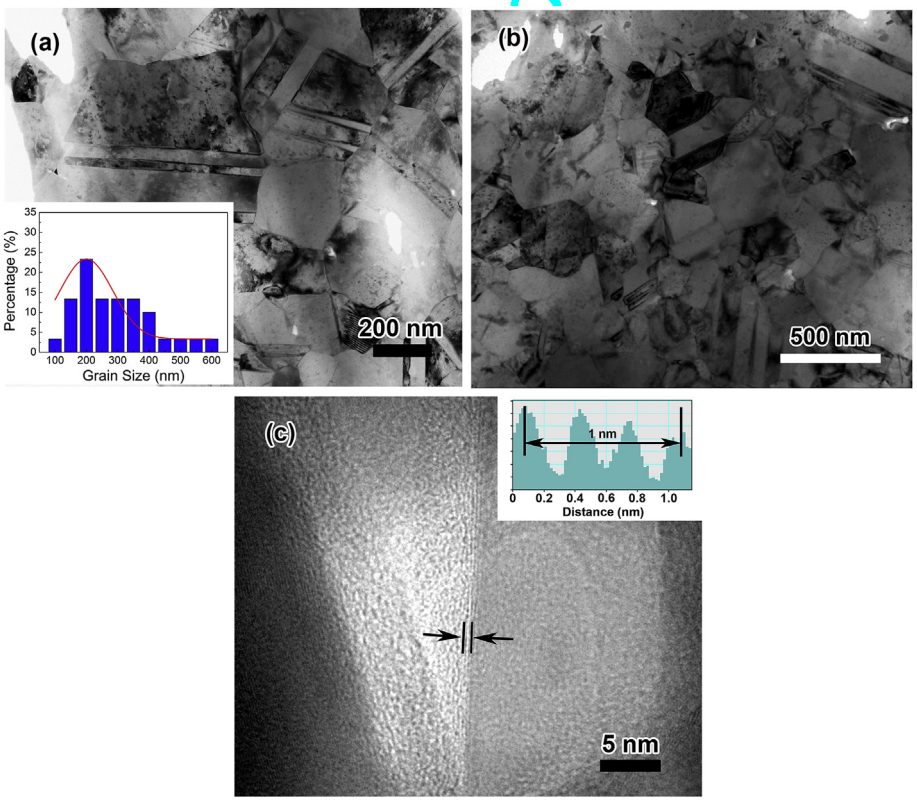

Fig. 7. (a) TEM image of the pure copper with the insert showing the statistic of grain size distribution in the pure copper, (b) TEM image of the 2.5G/Cu-20C-pH13.6(H) composite, (c) HRTEM image of the 2.5G/Cu-20C-pH13.6(H) composite. (A colour version of this figure can be viewed online.)

pure copper. It shows there are twin lamellar structures with a thickness ranging from 15 nm to 120 nm and the average Cu grain size is 200–300 nm (the inset of Fig. 7a). As shown in Fig. 7b, the nano grains and nano twins which have the similar size with the pure copper can be observed in the 2.5G/Cu-20C-pH13.6(H) composite and may contribute to the strengthening of the composites. The HRTEM image is shown in Fig. 7c. The edge of graphene sheet can be observed, which is about 3 layers and 1 nm in thickness. The

interlayer space of 0.334 nm, which is assigned to (111) plane of graphene [35].

Fig. 8 displays the fracture surfaces of RGO/Cu composites with different volume fraction of graphene (2.5 vol%, 5 vol% and 7.5 vol %). The fracture morphologies of the composites exhibit a dimple pattern which is a typical characteristic of plastic fracture. It can be seen that the fracture morphology of the 2.5G/Cu-20C-pH13.6(H) composite is extremely homogeneous and the dimples are about 500 nm in size in Fig. 9a. As the volume fraction of graphene increases, the size of the dimples is not consistent and keeps increasing due to graphene agglomerations (marked by yellow circles).

3.4. Mechanical and electrical properties of composites

Fig. 9a shows the true stress-strain curves of RGO/Cu composites fabricated at different pH values (6.6, 8.1 and 13.6). It can be seen that the fracture mode of the composite at pH 13.6 is plastic fracture and its ultimate tensile strength is as high as 748 MPa. However, when the pH value is below 8.1, the ultimate tensile strengths of the composites decrease greatly without obvious yielding stage from the stress-strain curves, which indicates that the fracture mode changed from plastic fracture to brittle fracture. This may be mainly attributed to the structure difference of the composites produced at different pH values. As above-mentioned, the composite particles are stable in the pH range of 5.9–9 and unstable in the pH range of 9–13.6. For the composites produced at pH 6.6 and 8.1 which contain large amount of $Cu_2(OH)_3Ac$ as shown in Fig. 2a, the composite particles repel each other to achieve stable dispersions in the solution and tend to produce a randomly distributed structure in the composites; however, for the composites produced at pH 13.6 which mainly contain $Cu(OH)_2$ sheets, the composite particles assemble and form hierarchical layered structure as above-mentioned. It has been reported that the layered structure contributes to the improvement of both the strength and toughness of composite [14,16]. Consequently, the composite fabricated at pH 13.6 has better mechanical properties than those composites fabricated at pH 6.6 and 8.1.

We can find that the reaction temperatures have remarkable effects on the tensile strengths and the elongations of the composites. The tensile strengths of the composites produced at room temperature, 40 °C and 50 °C are 748 MPa, 625 MPa and 288 MPa, respectively, as shown in Fig. 9a and b. With the increase of reaction temperature, the tensile strength decrease sharply from 748 MPa to 288 MPa. In addition, the tensile strength of composites with similar MLM process but fabricated at 80 °C is 355 MPa [19]. We can understand the phenomenon according to the different composite powder structures produced at different temperature as shown in Fig. 3. Copper compound particles produced at 20 °C and 40 °C have nano-layered structure, which combine easily with GO sheets and form hierarchical layered structure. However, when the reaction temperature reaches to 50 °C or higher, CuO nanoparticles are produced and easy to agglomerate as shown in Fig. 3d. This also results in the damage of the hierarchical layered structure.

The elongations of the composites are also affected by the reaction temperatures. The elongations of composite prepared by 20 °C, 40 °C and 50 °C are 1.45%, 1.04% and 0.20%, respectively. The direction of initial crack is forced to deviate from the initial propagation plane when it encounters the rigid hierarchical layered structure [36]. As a result, the hierarchical layered structure can cause the energy dissipation caused by the process of crack deflection [16,37–39].

We can find that high shear mixing contributes to the improvement of the dispersion of graphene and benefit the mechanical property of composite. High-shear mixing. In our previous work, high shear mixing can break through Van der Waals' force between layers and achieve the exfoliation of graphite [40]. With the help of high-shear mixing, the tensile strengths of the

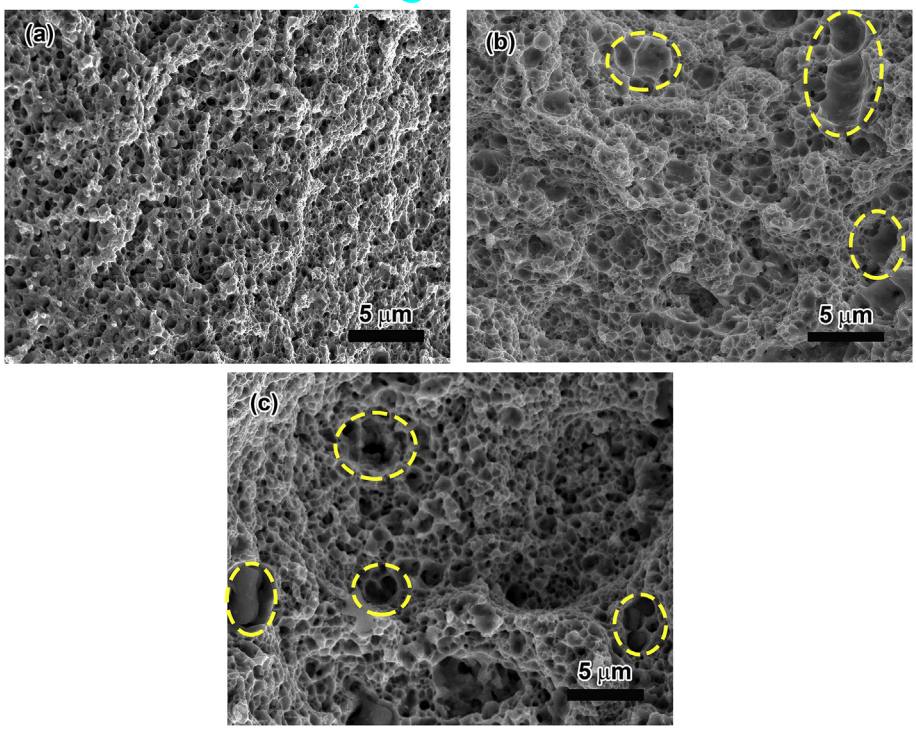

Fig. 8. SEM images for the fracture surface of RGO/Cu composites: (a) 2.5G/Cu-20C-pH13.6(H), (b) 5G/Cu-20C-pH13.6(H) and (c) 7.5G/Cu-20C-pH13.6(H). (A colour version of this figure can be viewed online.)

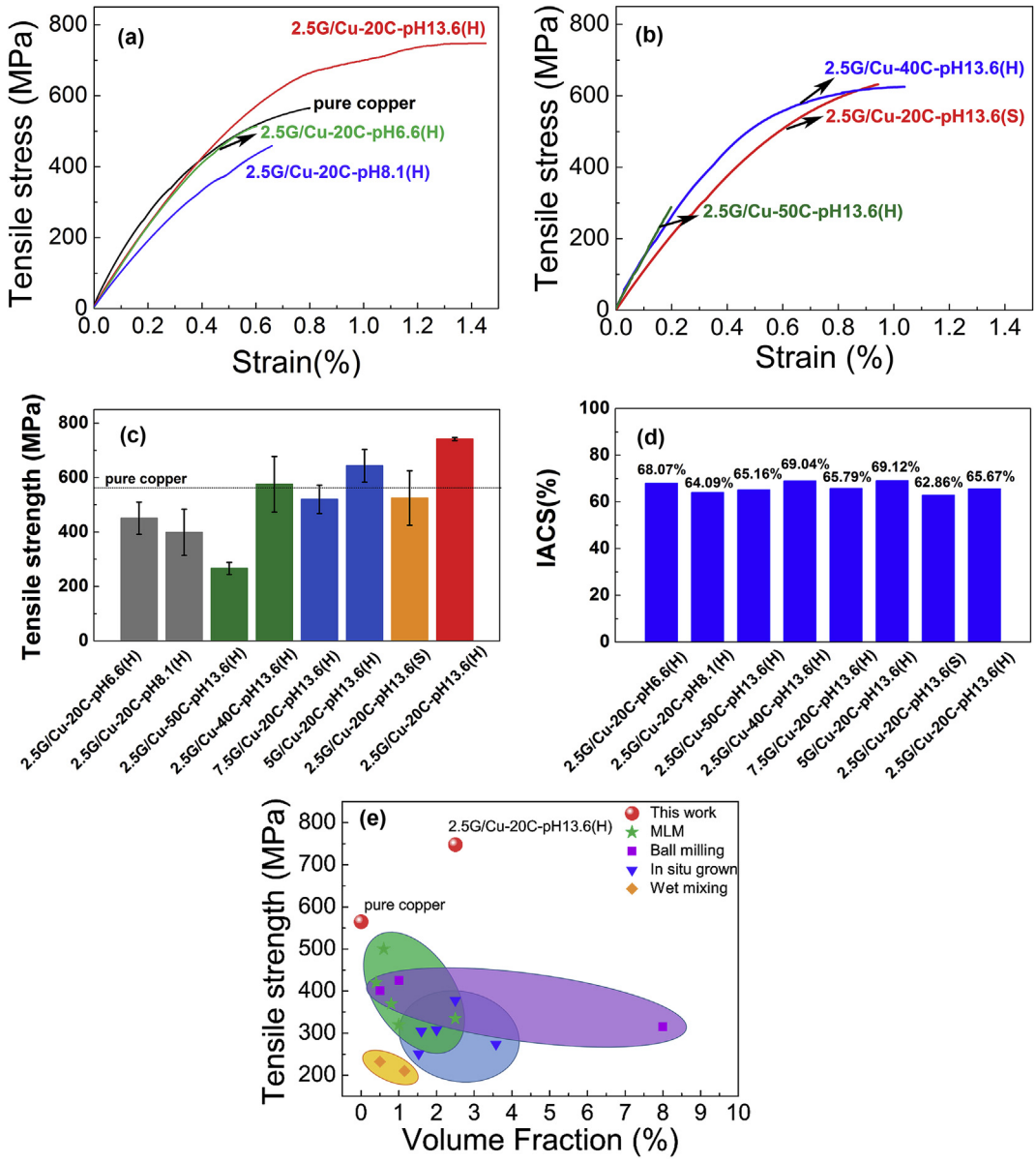

Fig. 9. (a) Tensile stress-strain curves of the pure copper and RGO/Cu composites at various pH values, (b) tensile stress-strain curves of RGO/Cu composites at various reaction temperatures and by mechanical stirring, (c) comparison of tensile strength of RGO/Cu composites in this work, (d) electrical conductivity of RGO/Cu composites in this work, (e) tensile strength versus reinforcement fraction of pure copper in this work and graphene/Cu composites. Note that the literature data are for graphene/Cu composites fabricated by various kinds of methods, including wet mixing (orange diamonds [44,45]), ball milling (purple squares [10,46]), conventional molecular level mixing (green stars [19,20]) and *in situ* grown (blue down triangles [47,48]). (A colour version of this figure can be viewed online.)

composites increase from 632 MPa to 748 MPa and the elongations increase from 0.95% to 1.45%. This results are in agreement with the SEM results in Fig. 5, which indicates that high shear mixing can produce more slender strips with larger length-width ratio than mechanical stirring.

For comparison, we have prepared a pure copper sample using the same method for the preparation of 2.5G/Cu-20C-pH13.6(H) composite. Fig. 9a also shows the true stress-strain curve of the pure copper sample. It is astonishing to find that the ultimate tensile strength is 565 MPa and the tensile yield strength is 470 MPa. The microstructure of the pure copper sample was observed by TEM as shown in Fig. 6a, which indicates that the pure copper has plenty of nano grains and nano twin lamellar structures. On the one hand, according to the traditional Hall-Petch relationship, for a pure copper with an average grain size of 200 nm, a yield strength of ~270 MPa is expected [41], which is much lower than that of the present sample in this work (470 MPa). On the other hand, twin boundary is a special kind of coherent boundary, which may effectively hinder dislocation motions [42]. Lu et al. [43] reported a copper sample with an average twin lamellar thickness of 80 nm has an ultrahigh yield strength of 500 MPa. Therefore, this result indicates that the high strength of the pure copper sample may be attributed to the strengthening effect of the nano-twins.

The comparison of all the ultimate tensile strengths of the RGO/Cu composites in this work are displayed for in Fig. 9c. It can be seen that the 2.5G/Cu-20C-pH13.6(H) composite has the highest tensile strength of 748 MPa with the smallest error bar compared with other samples. The tensile strength of the 2.5G/Cu-20C-pH13.6(H) composite is 183 MPa higher than that of the pure copper sample fabricated in the same condition. In addition, the effects of

graphene content on the mechanical property of RGO/Cu composite are also discussed. With the increase of graphene content, the tensile strength of RGO/Cu composites decrease from 748 MPa to 557 MPa. The main reason may be that the GO sheets tend to aggregate in the solution when the graphene content is high.

In addition, it is noting that the tensile strengths of some composites given in the present study, including 2.5G/Cu-20C-pH6.6(H), 2.5G/Cu-20C-pH8.1(H), 2.5G/Cu-50C-pH13.6(H), 7.5G/Cu-20C-pH13.6(H) and 2.5G/Cu-20C-pH13.6(S), are lower than the pure copper sample prepared in this work. It suggests that the formation of hierarchical layered structure plays a crucial role on the properties of the composites. The high strength can only be obtained in the composites prepared by the suitable technology parameters.

The electrical conductivity measurement of the composites was carried out by direct current method and expressed as the International Annealed Copper Standard (IACS). It can be found that the RGO/Cu composites in this work maintain a good electrical conductivity property between 62 %IACS and 70 %IACS, which indicates that the introduction of graphene does not weaken greatly the electrical conductivity of copper.

Fig. 9e shows the tensile strengths of graphene reinforced Cu matrix composites as a function of reinforcement amount by different methods. Obviously, the tensile strengths of the RGO/Cu composites with hierarchical layered structure go beyond any known graphene/Cu composites fabricated by other methods, verifying RGO/Cu composites with hierarchical layered structure have ultrahigh strength with low volume fraction. Furthermore, it is worth noting that the pure Cu with nano-twin structure in our study also exhibits higher strength. Although the exact reason should be clarified further, it is no doubt that the MLM method provided in the present study can be used to fabricate high strength copper.

4. Conclusion

In summary, hierarchical layered RGO/Cu composites are fabricated by MLM method and SPS process. For macroscale microstructure, the as-synthesized composites consist of carbon-rich strip phase and carbon-poor matrix. For microscale microstructure, the carbon-rich strip phases contain many micro-layered grains composing of alternating layers of graphene and copper. The unique hierarchical layered structure is realized by assembling GO/CuO_xH_y composite particles at pH value of 13.6 and temperature of 20 °C. In addition, high-shear mixing contributes to the formation of the hierarchical layered structure and the improvement of the dispersion of graphene in Cu matrix during the MLM process. The results show that excellent mechanical and electrical conductivity are simultaneously achieved in the RGO/Cu composites. Our work offers prospects for understanding the formation mechanism of hierarchical layered RGO/Cu composite, which can be promising for design, fabrication and optimization of graphene-based composites.

Acknowledgements

The authors gratefully acknowledge the support from Program of Qinghai Science and Technology Department (No. 2016-ZJ-701) and the National Natural Science Foundation of China (No.51671069 and 51301075).

References

[1] J.C. Meyer, A.K. Geim, M.I. Katsnelson, K.S. Novoselov, T.J. Booth, S. Roth, The structure of suspended graphene sheets, Nature 446 (7131) (2007) 60–63.
[2] C. Lee, X.D. Wei, J.W. Kysar, J. Hone, Measurement of the elastic properties and intrinsic strength of monolayer graphene, Science 321 (5887) (2008) 385–388.
[3] S. Stankovich, D.A. Dikin, G.H.B. Dommett, K.M. Kohlhaas, E.J. Zimney, E.A. Stach, et al., Graphene-based composite materials, Nature 442 (7100) (2006) 282–286.
[4] Y.W. Zhu, S. Murali, W.W. Cai, X.S. Li, J.W. Suk, J.R. Potts, et al., Graphene and graphene oxide: synthesis, properties, and applications, Adv. Mater. 22 (2010) 3906, 2010;22(46):5226-.
[5] A.K. Geim, Graphene: status and prospects, Science 324 (5934) (2009) 1530–1534.
[6] Y.B. Zhang, Y.W. Tan, H.L. Stormer, P. Kim, Experimental observation of the quantum hall effect and Berry's phase in graphene, Nature 438 (7065) (2005) 201–204.
[7] M.Y. Lim, H.J. Kim, S.J. Baek, K.Y. Kim, S.S. Lee, J.C. Lee, Improved strength and toughness of polyketone composites using extremely small amount of polyamide 6 grafted graphene oxides, Carbon 77 (2014) 366–378.
[8] Y.J. Wan, L.C. Tang, L.X. Gong, D. Yan, Y.B. Li, L.B. Wu, et al., Grafting of epoxy chains onto graphene oxide for epoxy composites with improved mechanical and thermal properties, Carbon 69 (2014) 467–480.
[9] J.Y. Wang, Z.Q. Li, G.L. Fan, H.H. Pan, Z.X. Chen, D. Zhang, Reinforcement with graphene nanosheets in aluminum matrix composites, Scr. Mater 66 (8) (2012) 594–597.
[10] W.J. Kim, T.J. Lee, S.H. Han, Multi-layer graphene/copper composites: preparation using high-ratio differential speed rolling, microstructure and mechanical properties, Carbon 69 (2014) 55–65.
[11] S.F. Bartolucci, J. Paras, M.A. Rafiee, J. Rafiee, S. Lee, D. Kapoor, et al., Graphene-aluminum nanocomposites, Mat. Sci. Eng. a-Struct. 528 (27) (2011) 7933–7937.
[12] S. Chen, L. Brown, M. Levendorf, W. Cai, S.Y. Ju, J. Edgeworth, et al., Oxidation resistance of graphene-coated Cu and Cu/Ni alloy, ACS Nano 5 (2) (2011) 1321–1327.
[13] P. Goli, H. Ning, X. Li, C.Y. Lu, K.S. Novoselov, A.A. Balandin, Thermal properties of graphene-copper-graphene heterogeneous films, Nano Lett. 14 (3) (2014) 1497–1503.
[14] Y. Kim, J. Lee, M.S. Yeom, J.W. Shin, H. Kim, Y. Cui, et al., Strengthening effect of single-atomic-layer graphene in metal-graphene nanolayered composites, Nat. Commun. 4 (2013).
[15] J. Liang, H. Bi, D. Wan, F. Huang, Novel Cu nanowires/graphene as the back contact for CdTe solar cells, Adv. Funct. Mater. 22 (6) (2012) 1267–1271.
[16] D.B. Xiong, M. Cao, Q. Guo, Z. Tan, G. Fan, Z. Li, et al., Graphene-and-copper artificial nacre fabricated by a preform impregnation process: bioinspired strategy for strengthening-toughening of metal matrix composite, ACS Nano 9 (7) (2015) 6934–6943.
[17] D.B. Xiong, M. Cao, Q. Guo, Z.Q. Tan, G.L. Fan, Z.Q. Li, et al., High content reduced graphene oxide reinforced copper with a bioinspired nano-laminated structure and large recoverable deformation ability, Sci. Rep. 6 (2016).
[18] S.I. Cha, K.T. Kim, S.N. Arshad, C.B. Mo, S.H. Hong, Extraordinary strengthening effect of carbon nanotubes in metal-matrix nanocomposites processed by molecular-level mixing, Adv. Mater. 17 (11) (2005) 1377. -+.
[19] J. Hwang, T. Yoon, S.H. Jin, J. Lee, T.S. Kim, S.H. Hong, et al., Enhanced mechanical properties of graphene/copper nanocomposites using a molecular-level mixing process, Adv. Mater. 25 (46) (2013) 6724–6729.
[20] F. Chen, J. Ying, Y. Wang, S. Du, Z. Liu, Q. Huang, Effects of graphene content on the microstructure and properties of copper matrix composites, Carbon 96 (2016) 836–842.
[21] L. Wang, Z. Yang, Y. Cui, B. Wei, S. Xu, J. Sheng, et al., Graphene-copper composite with micro-layered grains and ultrahigh strength, Sci. Rep. 7 (2017) 41896.
[22] N. Masciocchi, E. Corradi, A. Sironi, G. Moretti, G. Minelli, P. Porta, Preparation, characterization, and ab initio x-ray powder diffraction study of Cu-2(OH)(3)(CH_3COO)center dot H_2O, J. Solid State Chem. 131 (2) (1997) 252–262.
[23] B. Konkena, S. Vasudevan, Understanding aqueous dispersibility of graphene oxide and reduced graphene oxide through pK(a) measurements, J. Phys. Chem. Lett. 3 (7) (2012) 867–872.
[24] C.Q. Chen, Y.H. Zheng, Y.Y. Zhan, X.Y. Lin, Q. Zheng, K.M. Wei, Reduction of nanostructured CuO bundles: correlation between microstructure and reduction properties, Cryst. Growth Des. 8 (10) (2008) 3549–3554.
[25] J.P. Liu, X.T. Huang, Y.Y. Li, K.M. Sulieman, X. He, F.L. Sun, Self-assembled CuO monocrystalline nanoarchitectures with controlled dimensionality and morphology, Cryst. Growth Des. 6 (7) (2006) 1690–1696.
[26] B. Zhao, P. Liu, H. Zhuang, Z. Jiao, T. Fang, W.W. Xu, et al., Hierarchical self-assembly of microscale leaf-like CuO on graphene sheets for high-performance electrochemical capacitors, J. Mater Chem. A 1 (2) (2013) 367–373.
[27] K.T. Kim, S. Il Cha, T. Gemming, J. Eckert, S.H. Hong, The role of interfacial oxygen atoms in the enhanced mechanical properties of carbon-nanotube-reinforced metal matrix nanocomposites, Small 4 (11) (2008) 1936–1940.
[28] M. Park, B.H. Kim, S. Kim, D.S. Han, G. Kim, K.R. Lee, Improved binding between copper and carbon nanotubes in a composite using oxygen-containing functional groups, Carbon 49 (3) (2011) 811–818.
[29] Q. Zhang, C. Cai, J. Qin, B. Wei, Tunable self-discharge process of carbon nanotube based supercapacitors, Nano Energy 4 (2014) 14–22.
[30] Y. Shen, T. Jing, W. Ren, J. Zhang, Z.-G. Jiang, Z.-Z. Yu, et al., Chemical and

thermal reduction of graphene oxide and its electrically conductive polylactic acid nanocomposites, Compos. Sci. Technol. 72 (12) (2012) 1430–1435.
[31] D. Yang, A. Velamakanni, G. Bozoklu, S. Park, M. Stoller, R.D. Piner, et al., Chemical analysis of graphene oxide films after heat and chemical treatments by X-ray photoelectron and Micro-Raman spectroscopy, Carbon 47 (1) (2009) 145–152.
[32] A. Pulido, P. Concepción, M. Boronat, C. Botas, P. Alvarez, R. Menendez, et al., Reconstruction of the carbon sp_2 network in graphene oxide by low-temperature reaction with CO, J. Mater. Chem. 22 (1) (2012) 51–56.
[33] S. Pei, H.-M. Cheng, The reduction of graphene oxide, Carbon 50 (9) (2012) 3210–3228.
[34] K. Krishnamoorthy, M. Veerapandian, K. Yun, S.J. Kim, The Chemical and structural analysis of graphene oxide with different degrees of oxidation, Carbon 53 (2013) 38–49.
[35] M.Q. Zhao, Q. Zhang, J.Q. Huang, G.L. Tian, J.Q. Nie, H.J. Peng, et al., Unstacked double-layer templated graphene for high-rate lithium-sulphur batteries, Nat. Commun. 5 (2014).
[36] B. Wetzel, P. Rosso, F. Haupert, K. Friedrich, Epoxy nanocomposites - fracture and toughening mechanisms, Eng. Fract. Mech. 73 (16) (2006) 2375–2398.
[37] F. Bouville, E. Maire, S. Meille, B. Van de Moortele, A.J. Stevenson, S. Deville, Strong, tough and stiff bioinspired ceramics from brittle constituents, Nat. Mater. 13 (5) (2014) 508–514.
[38] U.G.K. Wegst, H. Bai, E. Saiz, A.P. Tomsia, R.O. Ritchie, Bioinspired structural materials, Nat. Mater. 14 (1) (2015) 23–36.
[39] E. Munch, M.E. Launey, D.H. Alsem, E. Saiz, A.P. Tomsia, R.O. Ritchie, Tough, bio-inspired hybrid materials, Science 322 (5907) (2008) 1516–1520.
[40] L. Wang, Y. Cui, S. Yang, B. Li, Y.Y. Liu, P. Dong, et al., Microstructure and properties of carbon nanosheet/copper composites processed by particle-assisted shear exfoliation, Rsc Adv. 5 (25) (2015) 19321–19328.
[41] M.A. Meyers, K.K. Chawla, Mechanical Metallurgy, Principles and Applications, Prentice-Hall, Englewood Cliffs, NJ, 1984, p. 496.
[42] J.W. Christian, S. Mahajan, Deformation twinning, Prog. Mater. Sci. 39 (1–2) (1995) 1–157.
[43] Y.F. Shen, L. Lu, Q.H. Lu, Z.H. Jin, K. Lu, Tensile properties of copper with nano-scale twins, Scr. Mater. 52 (10) (2005) 989–994.
[44] X. Gao, H.Y. Yue, E.J. Guo, H. Zhang, X.Y. Lin, L.H. Yao, et al., Mechanical properties and thermal conductivity of graphene reinforced copper matrix composites, Powder Technol. 301 (2016) 601–607.
[45] R.R. Jiang, X.F. Zhou, Z.P. Liu, Electroless Ni-plated graphene for tensile strength enhancement of copper, Mat. Sci. Eng. a-Struct 679 (2017) 323–328.
[46] K. Chu, C.C. Jia, Enhanced strength in bulk graphene-copper composites, Phys. Status Solidi 211 (1) (2014) 184–190.
[47] M. Yang, L. Weng, H. Zhu, T. Fan, D. Zhang, Simultaneously enhancing the strength, ductility and conductivity of copper matrix composites with graphene nanoribbons, Carbon 118 (2017) 250–260.
[48] Y. Chen, X. Zhang, E. Liu, C. He, C. Shi, J. Li, et al., Fabrication of in-situ grown graphene reinforced Cu matrix composites, Sci. Rep. 6 (2016) 19363.